01 Jan 1991

A Nuclear Fragmentation Energy Deposition Model

John W. Wilson
Missouri University of Science and Technology, jwilson@mst.edu

D. M. Ngo

T. N. Forgarty

W. W. Buck

A Nuclear Fragmentation Energy Deposition Model

D. M. Ngo, J. W. Wilson, T. N. Fogarty, *Associate Member, IEEE*, and W. W. Buck

***Abstract*—A formalism for target fragment transport is presented with application to energy loss spectra in thin silicon devices. A nuclear data base is recommended that agrees well with the measurements of McNulty *et al.* using surface barrier detectors. High-energy events observed by McNulty *et al.*, which are not predicted by intranuclear cascade models, are well represented by the present work.**

Introduction

THE early suggestion that some spacecraft anomalies may result from the passage of the galactic ions through microelectronic circuits [1] has now been well established. Although the direct ionization of protons appear as unlikely candidates, their nuclear reaction products are suspected as a source of single event upset (SEU) phenomena [2]–[4]. As a result, a number of fundamental experimental and theoretical studies were undertaken to better understand the phenomena. McNulty and co-workers measured the energy deposition of proton reaction products in Si using surface barrier detectors of various thickness from 2.5–200 μm [5]. They also developed a Monte Carlo code (OMNI) based on an intranuclear cascade model for theoretical evaluation of energy deposition from such products [5], [6]. A comparison of McNulty's intranuclear cascade model with the well established MECC7 code developed by Bertini and co-workers at Oak Ridge National Laboratory showed some differences in predicted reaction products and even greater differences in energy spectral contributions [7]. An evaluation of Si reaction products was likewise made by Petersen [4] and, although no direct comparison was made to McNulty's experiments, an estimate of SEU rates in the trapped proton environment was made.

More detailed applications to specific device geometry and parameter questions followed these fundamental studies. Bradford evolved an energy deposition formalism [8] using the cross sections of Hamm *et al.* [7]. McNulty *et al.* applied their Monte Carlo model to dynamic random access memory (DRAM) devices with reasonable success and discussed the implications of heavy-ion SEU phenomena on proton-induced SEU events through secondary reaction processes [9]. The fundamental consideration is the evaluation of the energy deposited within the sensitive volume of the device in question due to a passing proton. The ionization due to the proton makes only a small contribution to the critical charge. The illustration of the nuclear interaction in microelectronic device is shown in Fig. 1. Nuclear reaction events usually produce several reaction products (a heavy fragment and several lighter particles). As for the fragmentation process, a few heavy fragments may be produced simultaneously in certain events, yet all of the resultant products can make important contributions of the total energy deposited. Such nuclear events arise from a single nuclear reaction site and release kinetic energy to the produced particles in about 10^{-13} s. The kinetic energy of these products is deposited locally in the device material within 10^{-10} s so that the nuclear events strongly correlated in space and time.

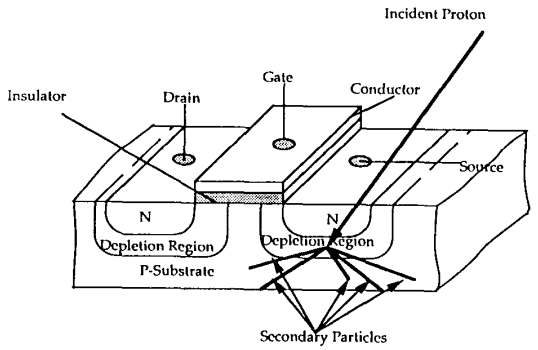

Fig. 1. Nuclear reaction taking place in N-MOS device.

There are three distinct approaches to a fundamental description of the energy deposition events. The first approach has been employed by McNulty and co-workers. They have developed a Monte Carlo code in which multiparticle events are calculated explicitly, including spatial and specific event (temporal) correlation effects. Although this is the most straight forward way of treating the full detail, it is a complex computational task. A second class of methods begins with the volumetric source of collision events and calculates the SEU probability using the chord length distribution [8], [10]. Although correlation effects could be so incorporated in principle, they appear to be ignored in both of the cited references. A third approach in which linear energy transfer (LET) distributions and chord length distributions are used seems most appropriate for external sources [11], [12]. This last approach applies if the LET distribution from external sources is constant over the sensitive volume; however, its applicability to volumetric sources is questionable. At the very least, this approach ignores correlation effects.

Nuclear data bases for biological systems were examined in [13]. The MECC7 results underestimated the energy transfer cross section for multiple charged ion products by nearly a factor of two. In a more detailed analysis, the Silberberg–Tsao fragmentation parameters appear to be superior to the MECC7 predicted cross sections [14]. The primary differences appear for the lighter of the multiple charged fragments. Further compari-

Manuscript received April 17, 1990; revised September 4, 1990. This work was supported in part by NASA grant NGT 50344.

D. M. Ngo is with the Physics Department, Old Dominion University, Norfolk, VA 23529.

J. W. Wilson is with NASA, Langley Research Center, Hampton, VA 23665.

T. N. Fogarty is with AT&T Bell Labs, 555 Union Blvd., Allentown, PA 18103.

W. W. Buck is with the Physics Department, Hampton University, Hampton, VA 23668.

IEEE Log Number 9040805.

0018-9499/91/0200-0002$01.00

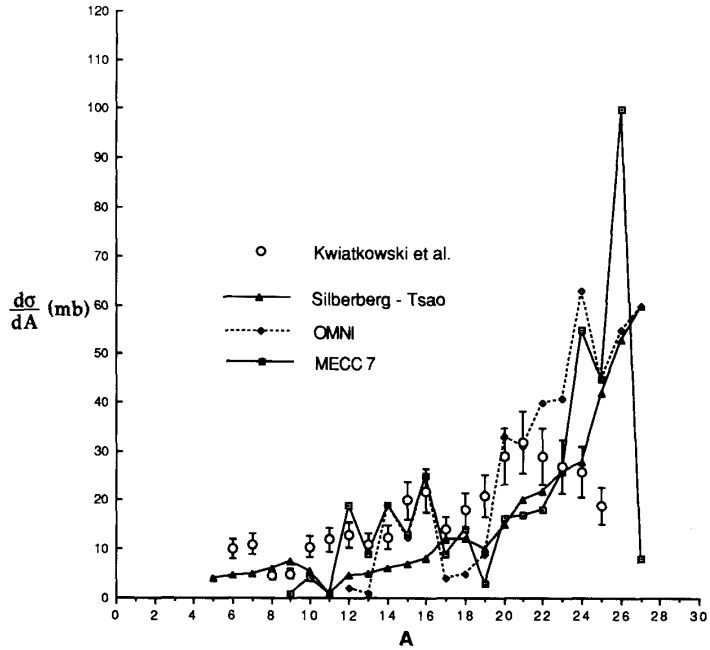

Fig. 2. Fragmentation cross section for 180-MeV protons on Al targets calculated by various models in comparison to experimental measurements.

son with experiments on Al targets shows that both Monte Carlo nuclear models (McNulty's code OMNI as well as the MECC7) tend to underestimate production cross sections for products lighter than fluorine in proton-induced reactions. Although these intranuclear cascade models are capable of representing multiparticle correlation, the inherent inaccuracies in predicting cross sections is a serious limitation.

In this present paper, the model for energy deposition in microelectronic devices is examined. Comparison of the present results with McNulty's experiments shows good agreement even for the high-energy events observed experimentally but not predicted by the Monte Carlo intranuclear cascade models.

Nuclear Fragmentation Cross Section

Although nuclear fragmentation has been under study for nearly 50 years, the absolute cross sections still stir some controversy. The experimental problem was that the main reaction products could be directly observed only in recent years and even now only in rather sophisticated experiments. Rudstam studied the systematics of nuclear fragmentation and supposed the fragment isotopes to be in a bell-shaped distribution about the nuclear stability line [16]. Silberberg and Tsao continued the Rudstam parametric approach and added many correction factors as new experimental evidence became available [12].

Concurrently, the Monte Carlo simulation of the Serber model [17] and final decay through compound nuclear models have shown some success [7], [18]. Even so, the Monte Carlo simulation of intranuclear cascades shows little success in predicting fragments whose mass is small compared with the original target nuclear mass [13], [19]. Of the various models for nucleon-induced fragmentation in ^{28}Si, the model of Silberberg and Tsao currently appears most reliable; jet computations are much simpler and faster than Monte Carlo codes by orders of magnitude [12]. The main limitation of their model is that only inclusive cross sections are predicted; on the other hand, particle correlations from the Silberberg and Tsao model could prove important in predicting SEU events.

Measurements of ^{27}Al fragmentation in proton beams have been made by Kwaitkowski *et al.* [19]. These experiments are compared in Fig. 2 to the Monte Carlo results of OMNI and MECC7. Also shown are the results of Silberberg and Tsao; generally, these results appear to be within a factor of 2 of the experiments. The model in [12] is the only model that predicts significant contributions in the important range below $A = 12$.

The spectrum of average recoil energy is calculated using the Silberberg–Tsao cross sections and compared with the spectrum according to the Bertini cross sections in Fig. 3. The Bertini cross section is a serious underestimate above 8 MeV and greatly overestimates below 3 MeV. Experimental evidence indicates that even the Silberberg–Tsao values are too small above 6 MeV in [19].

Nuclear Recoil Transport

In moving through bulk material, heavy ions give up energy to the medium through atomic/molecular and nuclear interaction. The heavy ions and struck nucleus produce secondary particles as fragments of the primary ion, which have longer ranges and free paths, causing much greater penetration than the primary ion. The continuous slowing-down theory is assumed here because of the energy loss as a result of the electromagnetic interaction with a small energy transfer. The transport equation of recoil target fragments is described as follows:

$$\left[\Omega \cdot \nabla - \frac{\partial}{\partial E} S_z(E)\right] \phi_z(x, \Omega, E) = \zeta_z(E) \qquad (1)$$

where $\phi_z(x, \Omega, E)$ is the ion flux in number of particles/cm^{2}s at x moving with motion along Ω and energy E in units of MeV; $S_z(E)$ is the linear energy transfer (LET) in MeV/cm; and $\zeta_z(E)$ is the ion source density in number of particles/cm^{3}s

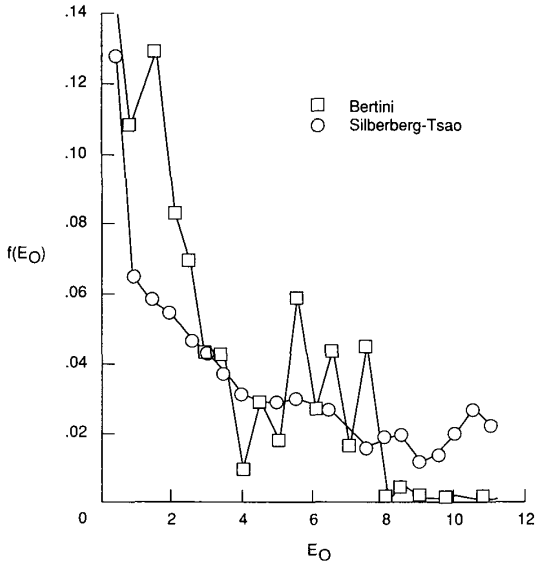

Fig. 3. Spectrum of average energy predicted by Silberberg-Tsao cross sections in comparison to Bertini cross sections.

and assumed to be isotropic and uniformly distributed through the media. The term on the left hand of (1) containing $S_z(E)$ is a result of the continuous slowing-down approximation, while the remaining terms of (1) are seen to be the usual Boltzmann terms.

The solution to (1) exists and is unique in any convex region for which the inbound flux of each ion type is specified everywhere on the bounding surface. The boundary condition is specified by requiring the solution of (1) to satisfy

$$\phi_z(\Gamma, \Omega, E) = F_z(\Omega, E), \qquad \text{for } \boldsymbol{n} \cdot \Omega < 0 \qquad (1a)$$

where $\boldsymbol{n}$ is the outward directed unit normal vector to the boundary surface.

The solution is found using the method of characteristics [20], [21] with a null boundary condition as

$$\phi_z(x, \Omega, E) = \frac{1}{S_z(E)} \int_E^{E_b} \zeta_z(E')\, dE'. \qquad (2)$$

If Γ is the point on the boundary determined by projecting x along in direction-Ω as shown in Fig. 4,

$$E_b = R_z^{-1}\left[R_z(E) + b\right] \qquad (3)$$

where

$$b = \Omega \cdot (x - \Gamma) \qquad (3a)$$

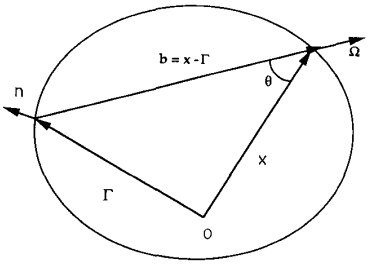

Fig. 4. Relation of boundary and vector quantities required for evaluation of ion fields.

and $R_z(E)$ is the range of ion. The distance traveled before coming to rest

$$R_Z(E) = \int_0^E \frac{dE'}{S_Z(E')}. \qquad (3b)$$

If an ion is known to come to rest in distance x, then its energy is found through the inverse of the previous relation as

$$E = R_z^{-1}(x). \qquad (4)$$

Equation (2) may be used to evaluate the spectrum of particles leaving the region that can be related to the spectrum of energy deposited in the media. An isolated sheet of silicon of thickness a, which is obviously similar to the McNulty surface barrier detectors, is considered. We first consider a monoenergetic ion source:

$$\zeta_z(E) = \frac{\sigma_z \phi}{4\pi} \delta(E - E') \qquad (5)$$

for which

$$\phi_z(x, \Omega, E) = \frac{\sigma_z \phi}{4\pi S_z(E)} \left\langle \begin{matrix} 1 & E \le E' \le E_b \\ 0 & \text{otherwise} \end{matrix} \right\rangle \qquad (6)$$

where σ_z is the silicon fragmentation cross section and ϕ the flux of initiating energetic particles. The spectrum of ions leaving the sheet (ignoring edge effects) is

$$\frac{df_z}{dE} = \int \phi_z(x, \Omega, E) \cos\theta\, d\Omega = 4\pi A \int_0^1 \phi_z(\Gamma, \Omega, E)\, \mu\, d\mu$$

$$= \frac{A\sigma_z\phi}{2S_z(E)} \left\langle \begin{matrix} \dfrac{a^2}{\{R_z(E') - R_z(E)\}^2}; & 0 \le E \le R_z^{-1}\left[R_z(E') - a\right] \\ 1; & R_z^{-1}\left[R_z(E') - a\right] \le E \le E' \\ 0; & E' < E \end{matrix} \right\rangle \qquad (7)$$

where A is the area of the sheet and μ is the cosine of the colatitude with respect to the local surface normal. The total number of ions that stop in the sheet is

$$N_s = Aa\sigma_z\phi \left\langle \begin{matrix} \left[\dfrac{a}{2R_z(E')}\right]; & a \le R_z(E') \\ \left[1 - \dfrac{R_z(E')}{2a}\right]; & a > R_z(E') \end{matrix} \right\rangle. \qquad (8)$$

Obviously, an ion produced with energy E' which leaves the sheet with energy E, suffered an energy loss ϵ to the sheet given by

$$\epsilon = E' - E \qquad (9)$$

which we use to find the energy loss spectrum as

$$\frac{df_{z\delta}}{d\epsilon} = \left(\frac{df_z}{dE}\right)_{E=E'-\epsilon} + N_s\delta(E'-\epsilon). \tag{10}$$

Considering that (10) is the energy deposition in a sheet of area A and thickness a as the result of a mono-mono-energetic volumetric source, the response to any arbitrary spectral source can be found by superposition.

Fragmentation Energy Loss Spectra

The fragmentation source energy distribution (normalized to unity) is given as

$$\rho(E') = \left(\sqrt{\frac{E'}{2\pi E_0^3}}\right)\exp\left(\frac{-E'}{2E_0}\right) \tag{11}$$

where $3E_0$ is the mean fragment energy that depends on fragment mass and is given by Wilson *et al.* [14] based on earlier work of Goldhaber [22].

The energy loss spectrum is found using (10) and (11) as

$$\frac{dF}{d\epsilon} = \int_\epsilon^\infty \left(\frac{df_{z\delta}}{d\epsilon}\right)_{E=E'-\epsilon}\rho(E')\,dE' = \int_0^\infty \left(\frac{df_{z\delta}}{d\epsilon}\right)_{E'=E+\epsilon}\rho(E+\epsilon)\,d. \tag{12}$$

The contribution from stopping ions is readily evaluated to give

$$\frac{dF}{d\epsilon} = N_S(\epsilon)\rho(\epsilon)\int_0^\infty \left(\frac{df_z\delta}{d\epsilon}\right)_{E'=E+\epsilon}\rho(E+\epsilon)\,dE. \tag{13}$$

The second term of (13) is divided into three subintervals as

$$I_1(\epsilon) = \int_0^{E_2}\left(\frac{df_z}{d\epsilon}\right)_{E'=E+\epsilon}\rho(E+\epsilon)\,dE \tag{13.1}$$

$$I_2(\epsilon) = \int_{E_2}^{E_1}\left(\frac{df_z}{d\epsilon}\right)_{E'=E+\epsilon}\rho(E+\epsilon)\,dE \tag{13.2}$$

$$I_3(\epsilon) = \int_{E_1}^{\infty}\left(\frac{df_z}{d\epsilon}\right)_{E'=E+\epsilon}\rho(E+\epsilon)\,dE. \tag{13.3}$$

First, $I_1(\epsilon)$ is zero unless $R_z(\epsilon) > 2a$, for which

$$I_1(\epsilon) = \frac{A\sigma_z\phi}{2}\left\{\frac{a^2}{R_z^2(\epsilon)}P(E_2,\epsilon) + \left[\frac{1}{4} - \frac{a^2}{R_z^2(\epsilon)}\right]\frac{Q(E_2,\epsilon)}{R_z(E_2)}\right\} \tag{14}$$

$$I_2(\epsilon) = \frac{A\sigma_z\phi}{2}\left\{\left[\frac{1}{4} - \frac{3}{4}\frac{R_z(E_2)}{[R_z(E_1)-R_z(E_2)]}\right\}\cdot[P(E_1,\epsilon)-P(E_2,\epsilon)] + \frac{A\sigma_z\phi}{2}\frac{3}{4}\left[\frac{Q(E_1,\epsilon)-Q(E_2,\epsilon)}{[R_z(E_1)-R_z(E_2)]}\right] \tag{15}$$

$$I_3(\epsilon) = \frac{A\sigma_z\phi}{2}\int_{E_1}^\infty \frac{\rho(E+\epsilon)}{S_z(E)}\,dE \tag{16}$$

with $R_z(E_2) = R_z(E_2+\epsilon) - 2a$ and $R_z(E_1) = R_z(E_1+\epsilon) - a$. If $a \le R_z(\epsilon) \le 2a$, then E_2 and $I_1(\epsilon)$ are equal to zero:

$$I_2(\epsilon) = \frac{A\sigma_z\phi}{2}\left\{\frac{a^2}{R_z^2(\epsilon)}P(E_1,\epsilon) + \left[1 - \frac{a^2}{R_z^2(\epsilon)}\right]\frac{Q(E_1,\epsilon)}{R_z(E_1)}\right\}. \tag{17}$$

When $R_z(\epsilon) \le a$, then $E_1 = E_2 = 0$, so that $I_1(\epsilon)$ and $I_2(\epsilon)$ both vanish and

$$I_3(\epsilon) = \frac{A\sigma_z\phi}{2}\int_0^\infty \frac{\rho(E+\epsilon)}{S_z(E)}\,dE. \tag{18}$$

In (14), (15), and (17), P and Q are given by

$$P(E_i,\epsilon) = \int_0^{E_i}\frac{\rho(E+\epsilon)}{S_s(E)}\,dE \tag{19}$$

$$Q(E_i,\epsilon) = \int_0^{E_i}\frac{R_z(E)\rho(E+\epsilon)}{S_s(E)}\,dE. \tag{20}$$

The integral of (19) may be approximated for values of $E_i \le 1/4(\epsilon)$ by

$$P(E_i,\epsilon) \cong \frac{R_z(E_0)}{\sqrt{2}}\rho(\epsilon)\left\{\frac{1}{2}\gamma\left(\frac{1}{2},\frac{E_i}{2E_0}\right)\right. \tag{21}$$

where γ is an incomplete gamma function. For larger values of E_i such that $1/4(\epsilon) \le E_i \le 4\epsilon$, the integral may be taken as

$$P(E_i,\epsilon) \cong \frac{R_z(E_0)}{\sqrt{2}}\rho(\epsilon)\cdot\left\{\frac{1}{2}\gamma\left(\frac{1}{2},\frac{\epsilon}{8E_0}\right) + \frac{1}{2}\gamma\left(\frac{1}{2},\frac{E_i}{2E_0}\right) + \sqrt{\frac{2E_0}{\epsilon}}\gamma\left(1,\frac{E_i}{2E_0}\right) - \sqrt{\frac{2E_0}{\epsilon}}\gamma\left(1,\frac{\epsilon}{8E_0}\right)\right\}. \tag{22}$$

Whenever $E_i > 4\epsilon$, the integral is approximately

$$P(E_i,\epsilon) \cong \frac{R_z(E_0)}{\sqrt{2}}\rho(\epsilon)\cdot\left\{\frac{1}{2}\gamma\left(\frac{1}{2},\frac{\epsilon}{8E_0}\right) + \frac{1}{2}\gamma\left(\frac{1}{2},\frac{4\epsilon}{2E_0}\right) + \sqrt{\frac{2E_0}{\epsilon}}\gamma\left(1,\frac{E_i}{2E_0}\right) - \sqrt{\frac{2E_0}{\epsilon}}\gamma\left(1,\frac{\epsilon}{8E_0}\right)\right\}. \tag{23}$$

The integral in (20) may be approximated by

$$Q(E_i,\epsilon) \approx \frac{R_z^2(E_0)}{2E_0}[C(E_i+\epsilon) - C(\epsilon)] \tag{24}$$

where $C(\epsilon)$ is the integral spectrum

$$C(E) = \int_0^E \rho(E')\,dE'. \tag{25}$$

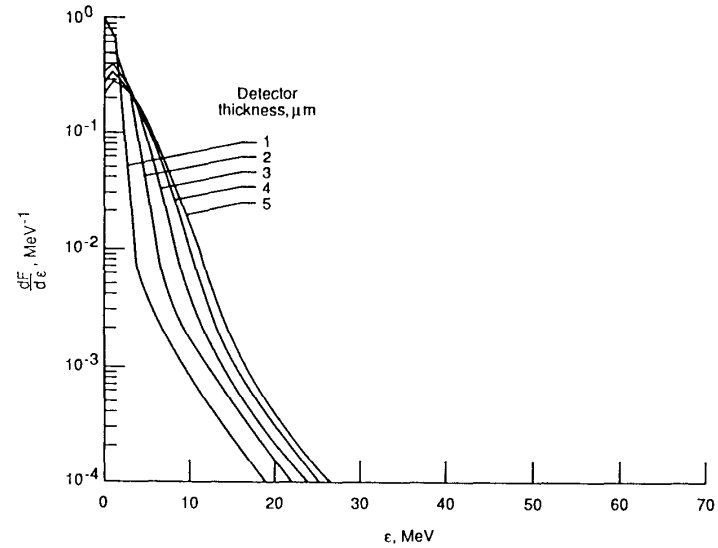

Fig. 5. Total absorption spectrum for surface barrier detector of 1–5 μm and $E_0 = 3.5$ MeV.

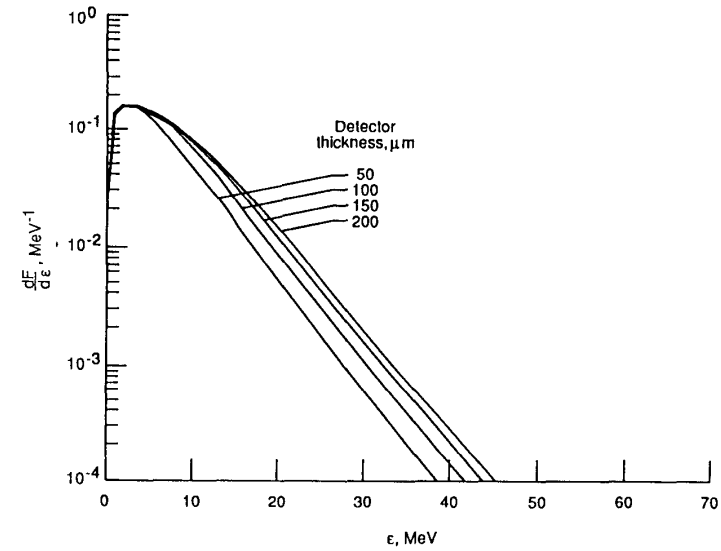

Fig. 6. Total absorption spectrum for surface barrier detector of 5–200 μm and $E_0 = 3.5$ MeV.

The total absorption spectrum is then

$$\frac{dF}{d\epsilon} = N_S(\epsilon)\rho(\epsilon) + I_1(\epsilon) + I_2(\epsilon) + I_3(\epsilon) \qquad (26)$$

and is shown in Fig. 5 for detector thickness of 1–5 μm with $E_0 = 3.5$ MeV. Similar results are shown in Fig. 6 for detector thickness of 20–200 μm. In comparing Figs. 5 and 6, it is shown that the energy loss spectrum is approaching the fragment-production spectrums as the thickness a becomes larger. There is an energy loss spectrum for each fragment produced that must be summed to obtain the total detector response.

Results

Typical fragmentation cross sections calculated using Silberberg–Tsao are shown in Table I for 125 MeV protons. The values of E_0 are taken from [14]. The calculated response of the 2.5-μm detector is shown in Fig. 7 as the crosses; these values should be compared with the experiments of McNulty and the values according to the Monte Carlo code of the McNulty group, which are also shown in Fig. 7. The peak value at zero energy is fixed by the total reaction cross section and total proton flux. It appears that the total reaction cross section of the Monte Carlo code is too small. Otherwise, the present theory and the Monte Carlo code show nearly equivalent agreement with the experi-

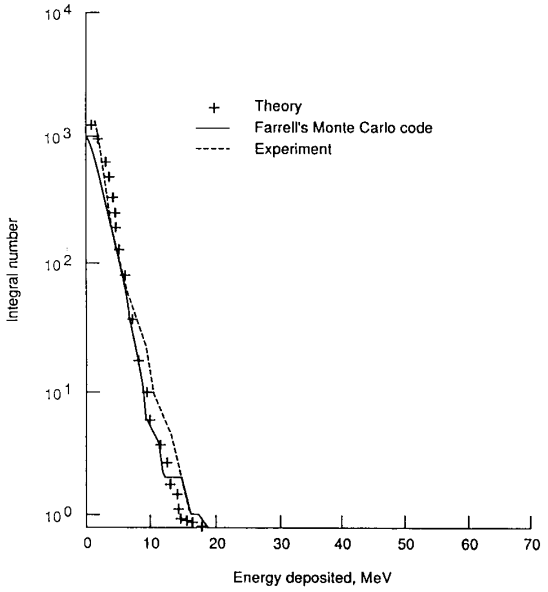

Fig. 7. Response of 2.5-μm surface barrier detector to 125-MeV protons ($2.14 \cdot 10^8$).

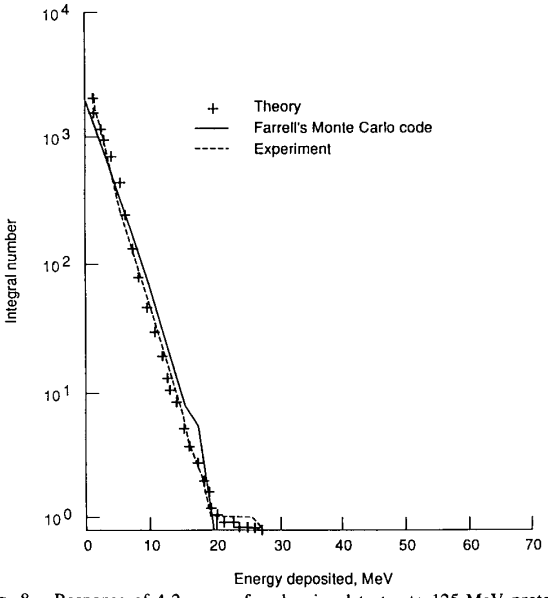

Fig. 8. Response of 4.2-μm surface barrier detector to 125-MeV protons ($2.14 \cdot 10^8$).

ments. Similar comments apply to the 4.2-μm detector response (Fig. 8) with one exception. The energetic events above 20 MeV observed in experiments are well represented by the present theory but not by the Monte Carlo code as expected by observing Fig. 3. This high-energy agreement between the present theory is observed for the 24.1-μm detector, but the Monte Carlo code again fails to predict the high-energy events as shown in Fig. 9. The improved model of the present work is again clearly displayed for the 158-MeV experiments of McNulty *et al.* as shown in Figs. 10 and 11.

The inability of the Monte Carlo codes to predict the most energetic fragments could be a serious limitation in predicting

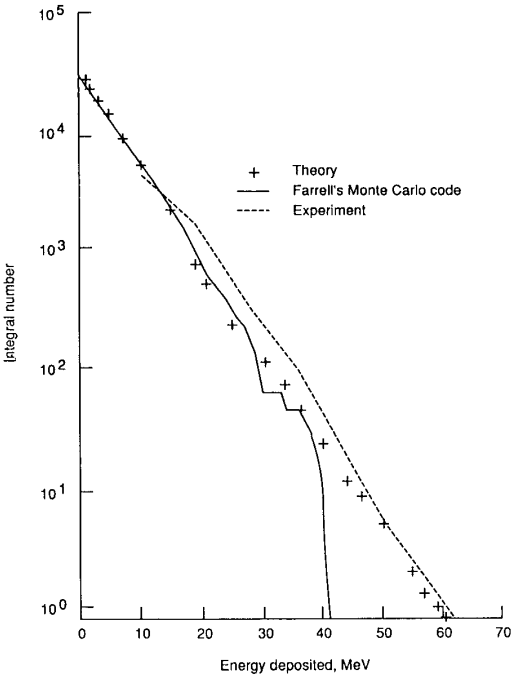

Fig. 9. Response of 2.5-μm surface barrier detector to 125-MeV protons ($6.42 \cdot 10^8$).

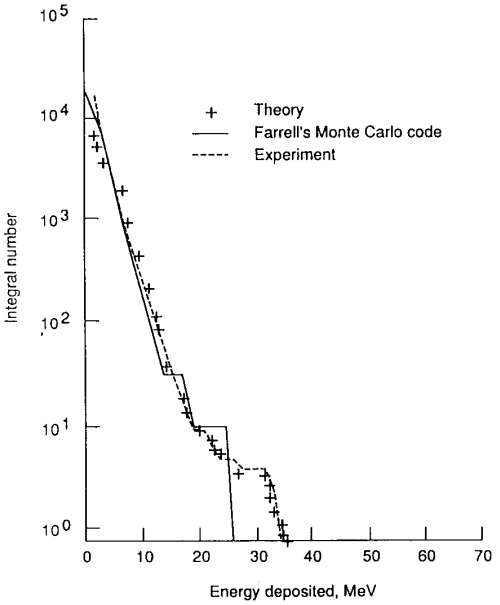

Fig. 10. Response of 2.5-μm surface barrier detector to 158-MeV protons ($3.9 \cdot 10^9$).

SEU in some devices. Although the Silberberg–Tsao cross sections for proton-induced reactions are not in complete agreement with some recent cross section measurements, they still provide improved ability over Monte Carlo models. The methods of analysis used in this paper will be applied to specific device geometries in the near future.

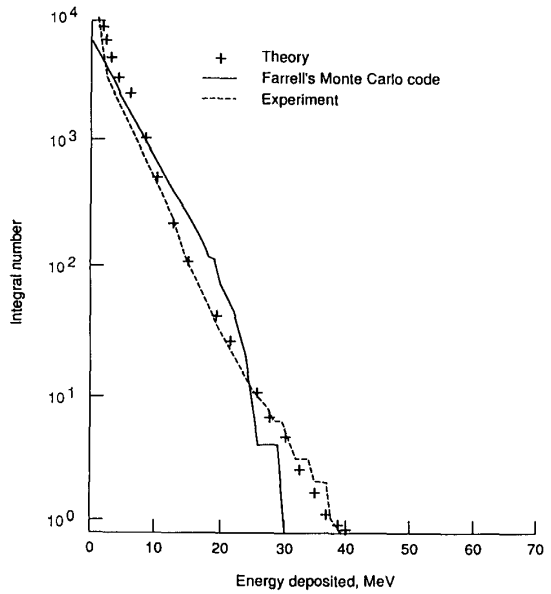

Fig. 11. Response of 8.7-μm surface barrier detector to 158-MeV protons ($3.9 \cdot 10^9$).

TABLE I
CROSS SECTION PARAMETERS FOR THE FRAGMENTATION OF ^{28}Si BY 125-MeV PROTONS

A_F	σ_F	E_0 (MeV)
27	67.7	0.17
26	50.8	.34
25	44.5	.50
24	37.7	.67
23	24.7	.84
22	24.5	1.01
21	14.7	1.17
20	15.3	1.34
19	8.1	1.51
18	7.3	1.68
17	6.4	1.85
16	6.1	2.01
15	4.2	2.18
14	2.9	2.35
13	1.9	2.52
12	2.3	2.68
11	1.5	2.85
10	1.0	3.02
9	1.1	3.19
8	1.7	3.35
7	1.9	3.52
6	1.5	3.69
5	1.2	3.86
4	145.9	2.08
3	29.1	2.92
2	70.7	2.13
1	710.5	2.06

REFERENCES

[1] D. Binder, E. C. Smith, and A. B. Holman, "Satellite anomalies from galactic cosmic rays," *IEEE Trans. Nucl. Sci.*, vol. NS-25, no. 6, pp. 2675–2680, Dec. 1975.

[2] R. C. Wyatt, P. J. McNulty, P. Toumbas, P. L. Rothwell, and R. C. Filtz, "Soft errors induced by energetic proton," *IEEE Trans. Nucl. Sci.*, vol. NS-26, no. 6, pp. 4905–4910, Dec. 1979.

[3] C. S. Guenzer *et al.*, "Single event upsets in RAMs induced by protons at 4.2 GeV and protons and newtrons below 100 MeV," *IEEE Trans. Nucl. Sci.*, vol. NS-27, no. 6, pp. 4985–4989, Dec. 1980.

[4] E. L. Petersen, "Nuclear reaction in semiconductor," *IEEE Trans. Nucl. Sci.*, vol. NS-27, no. 6, pp. 1485–1489, Dec. 1980.

[5] P. J. McNulty *et al.*, "Upset phenomena induced by energetic protons and electrons," *IEEE Trans. Nucl. Sci.*, vol. NS-27, no. 6, pp. 1516–1520, Dec. 1980.

[6] P. J. McNulty, G. E. Farrell, and W. P. Tucker, "Proton induced nuclear reactions in silicon," *IEEE Trans. Nucl. Sci.*, vol. NS-28, no. 6, pp. 4007–4012, Dec. 1981.

[7] R. N. Hamm, M. L. Rustgi, H. A. Wright, and J. E. Turner, "Energy spectra of heavy fragments from the interaction of protons with communications materials," *IEEE Trans. Nucl. Sci.*, vol. NS-28, no. 6, pp. 4004–4006, Dec. 1981.

[8] J. N. Bradford, "Microvolume energy deposition from high energy proton–silicon reactions," *IEEE Trans. Nucl. Sci.*, vol. NS-29, no. 6, pp. 2085–2089, Dec. 1982.

[9] J. M. Bisgrave *et al.*, "Comparison of soft errors induced by heavy ions and protons," *IEEE Trans. Nucl. Sci.*, vol. NS-33, no. 6, pp. 1571–1576, Dec. 1986.

[10] K. W. Fernald and S. E. Kerns, "Simulation of proton induced energy deposition in integrated circuits," *IEEE Trans. Nucl. Sci.*, vol. NS-35, no. 1, 981–986, Feb. 1988.

[11] E. L. Petersen, P. Shapiro, J. H. Adams, and E. A. Burke, "Calculation of cosmic-ray induced soft upsets and scaling of VLSI devices," *IEEE Trans. Nucl. Sci.*, vol. NS-29, no. 6, pp. 2055–2063, Dec. 1982.

[12] R. Silberberg and C. H. Tsao, "Cosmic ray transport in the atmosphere: Dose and LET—Distributions in materials," *IEEE Trans. Nucl. Sci.*, vol. NS-30, no. 6, pp. 4398–4404, Dec. 1983.

[13] J. W. Wilson, S. Y. Chun, W. W. Buck, and L. W. Townsend, "High energy nucleon data bases," *Health Physics*, vol. 55, pp. 817–819, Nov. 1988.

[14] J. W. Wilson *et al.*, "BRYNTRN: A baryon transport model," in NASA TP 2887, 1989.

[15] J. H. Chern, J. A. Seichik, and P. Yang, "Single event charge collection in CMOS multi-junctions structure," in *1986 Int. Electron Dev. Meeting – Tech. Digest.*, IDEM 86, pp. 538–541, 1986.

[16] G. Rudstam, "Systematic of spallation yields," *Zeitschrift fur Naturforschung*, vol. 21a, pp. 1027–1041, Jul. 1966.

[17] R. Serber, "Nuclear reactions at high energies," *Phys. Rev.*, vol. 72, no. 11, pp. 1114–1115, Dec. 1947.

[18] H. W. Bertini, "Intranuclear-cascade of the secondary nucleon spectra from nucleon–nucleus interactions in the energy range 340 to 2900 MeV and comparisons with experiment," *Phys. Rev.*, vol. 188, no. 4, pp. 1711–1730, 1969.

[19] K. Kwaitkowski, S. H. Zhou, T. E. Ward, and V. E. Viola, Jr., "Energy deposition in intermediate-energy nucleon–nucleus collisions," *Phys. Rev. Lett.*, vol. 50, no. 21, pp. 1648–1651, 1983.

[20] J. W. Wilson and S. L. Lamkin, "Perturbation theory for charged-particle transport in one dimension," *Nucl. Sci. Eng.*, vol. 57, no. 4, pp. 292–299, Aug. 1975.

[21] J. W. Wilson, "Analysis of the theory of high energy ion transport," in NASA TN D-8381, 1977.

[22] A. S. Goldhaber, "Statistical models of fragmentation processes," *Phys. Lett.*, vol. 53B, no. 4, pp. 306–308, Dec. 1974.